QR – Issue

QR – Article

Etse Dablu Bobobee
School of Information Engineering, Southwest University of Science and Technology (SWUST)
B. Ed IT, M. Eng. Info. & Com., PhD. student
Mianyang 621010, Sichuan China
bobosonj@gmail.com

Shunli Wang
School of Information Engineering (SWUST)
Dr., Professor Head of DTLab
497420789@qq.com

Chun-Mei Yu
School of Information Engineering (SWUST)
Dr., Professor

Chuanyun Zou
School of Information Engineering (SWUST)
Dr., Professor

Emmanuel Appiah
School of Information Engineering (SWUST)
PhD. student

Cong Jiang
School of Information Engineering (SWUST)
Master's student

Mingfang He
School of Information Engineering (SWUST)
Master's student

STATE OF CHARGE ESTIMATION OF HIGH-POWER LITHIUM-ION BATTERIES WITH IMPROVED EQUIVALENT CIRCUIT MODELING AND ADAPTIVE EXTENDED KALMAN FILTERING ALGORITHM

Abstract: This paper focuses on the accurate estimation of the state of charge of lithium-ion batteries through the establishment of an equivalent model, experimentation, simulation, and the use of an adaptive extended Kalman filtering algorithm. Several models have been used in the creation of the high-power lithium-ion battery and as it is difficult to estimate the state of charge of the lithium-ion battery accurately numerous methods and techniques are employed. A Thevenin equivalent circuit model is designed to include two resistor-capacitors in series for easy parameterization and estimation of the state of charge of the battery. An experimental approach is adopted and data from the open-circuit voltage and the hybrid pulse power characteristic tests are used for parameterization. The battery is modeled and simulated in Simulink/MATLAB with inputs from the results and calculations from the experimental data. An improved adaptive extended Kalman filtering algorithm was used to accurately estimate the state of charge. The main idea of using the improved adaptive algorithm is to update the statistical noise covariance parameters and to improve the estimation performance and accuracy. This reduced the interference of system noise

Clarivate
Analytics **indexed**

effectively and minimized estimation error to the smallest value. An extended Kalman filtering algorithm was employed alongside the adaptive extended Kalman filtering algorithm to verify the effectiveness of the adaptive algorithm. Results and computations from the experiment and simulation are compared and the results show that the improved adaptive extend Kalman filtering algorithm has good convergence speed, is more stable, and has a high precision of accuracy in the estimation of the state of charge. The maximum estimation error realized with the use of the extended Kalman filtering algorithm was 4.97%, and the maximum estimation error based on the use of the improved adaptive extended Kalman filtering algorithm was 1.85%. The results, therefore, show that the adaptive algorithm adopted in this paper can be used efficiently and effectively for the accurate state of charge estimation of the high-power lithium-ion battery.

Introduction

Currently, lithium-ion batteries are perhaps the most important new energy source in the 21st century, and research in the area of improving and enhancing the performance of the technology through various techniques and methods is key to unearthing greater potential. The key to improving, controlling, monitoring, and managing the lithium-ion battery is the battery management system (BMS) [1], and the estimation of the state of charge (SOC), state of health (SOH), state of power (SOP), and other battery parameters is a very important research field that ensures the safety and reliability of electronic devices that use these batteries as a source of power. Research on the improvement of the function, reliability, and performance of lithium-ion battery technology is important and any breakthrough in the area would go a long way to improve upon the technology [2]. The BMS is responsible for measuring the states of the battery accurately and also ensure safe operation and prolong the battery life [3]. An improved Thevenin equivalent circuit model was proposed, designed, and implemented through experimentation and simulation. The model was achieved by adding an extra RC branch to the Thevenin model, making it a second-order resistor-capacitor. The 2RC Thevenin model has better accuracy, stability, robustness, and is very effective for SOC estimation [4]. This model was used to study and record parameters and estimate relationships between voltage, current, SOC, and the charging/discharging characteristics.

Research concerning battery management systems (BMS) from a global perspective includes those which display an entire BMS design adopting a distributed structure to reach better scalability and portability [5]. Different approaches to designing a BMS depend on the functionalities desired for the specific application, but most of them focus on key functions such as SOC estimation [6] and the balancing process [7]. The improvement is towards the design of intelligent BMS's for electric and hybrid electric vehicles [8], and artificial intelligence applied for the battery state estimation [9]. SOC estimation has therefore drawn the attention of many researchers, and many different methods have been proposed [10, 11]. The OCV method, a full charge detector/dynamic load observer, and the CC method with robust extended Kalman filtering algorithm (REKF) are combined in [12]. It is difficult to determine the specific approach when such methods are used, however, based on the classification made in [12, 13], two categories; direct and indirect methods, and several subcategories that summarize trends in SOC estimation are mentioned and aligned appropriately.

Battery models are used to study the relationship between the external characteristics and the internal states of a battery by establishing a mathematical model. Models in a discrete-time state-space form are also used for SOC estimation [14, 15]. Current literature makes mention of the use of equivalent circuit models (ECMs) as being widely used as a foundation for model-based estimation and control [16]. Generally, equivalent circuit models including the Rint model, the Thevenin model, the RC model, and the partnership for a new generation of vehicle (PNGV) model [17] are selected. The first-order RC, second-order RC, and third-order RC are all employed to accurately model the battery [18, 19]. Among them, the Thevenin model is widely used, but not accurate enough since all of its elements can change, depending on the condition and state of the battery.

According to [20, 21], to maximize parameter identification, new designs are being developed using charging/discharging, and [22, 23] combined SOC estimation methods as a means of estimating SOC in the presence of unknown or time-varying battery parameters. Research in the area either assumes an accurate SOC/OCV relationship or seeks to impose approximations such as OCV being piece-wise linear with SOC [24] or constant during discharging [25]. According to [11, 26], RC parameters are determined through analyzing the transients in a battery voltage

Clarivate Analytics *indexed*

response under certain excitations such as constant or pulse current experiments. The voltage source in an ECM typically represents the battery's open-circuit voltage, which depends on the SOC [27]. A relationship between SOC and OCV can be identified by charging or discharging the battery using a small current [28]. Parameter identification based on current-voltage data is addressed in [21], by a method that reduces the problem of solving a set of high-order polynomial equations into solving several linear equations and a single-variable polynomial equation. A Thevenin ECM is used in [14] for every single cell in an array of more than 90 series-connected cells, to identify the internal resistance of each cell. In [29] a Thevenin model using two different branches for charge and discharge is connected in series n times to represent n cells in a series. According to [30, 31], there are three different ECMs of lithium-ion batteries widely adopted because of their excellent dynamic performance and postulates that the second-order ECM is the most accurate and has the best dynamic performance, but it is also the most complex. The Thevenin model and second-order ECM were used for SOC estimation and compared with three other enhanced ECMs in [14, 32] and the difference between these models is the way the SOC equations are calculated. The parameters of the second-order ECM can be calculated with different datasets depending on the purpose, like in [33]. In [34], a comparison between continuous-time and discrete-time equations of the second-order ECM is made and concludes that discrete-time identification methods are less robust due to undesired sensitivity issues in the transformation of discrete domain parameters.

According to [35], SOC can be directly calculated by the transformation of model equations with the deployment of a simple Thevenin ECM. In [36], a Thevenin ECM is used to obtain the OCV, and then, a linear fitting of a portion of the OCV–SOC curve is used to obtain the SOC. A similar process is used in [37] to obtain the SOC with a simple ECM that considers just a voltage source and an internal resistance. A Kalman filter (KF) is introduced in [38] to extract an OCV value in a noisy environment, and then to estimate SOC based on the OCV–SOC mapping. In addition to models, there are different types of closed-loop methods for SOC estimations, such as direct feedback [13], extended Kalman Filters [39], unscented Kalman Filters (UKF) [40, 41], and neural network [42, 43]. These methods are used to further improve the accuracy of the SOC estimation since they can recursively estimate the uncertainty of system state estimations and adapt Kalman gain to achieve optimal estimation in the next time step of the iteration process. It is common to find a combination of CC or OCV methods with the KF method like in [44, 45] and as proposed in [46, 47], the EKF method is also used in combination with CC and/or OCV. Another common improvement to the Kalman

filtering algorithm for SOC estimation is the unscented Kalman filtering algorithm, which is used in [48, 49] to improve estimation accuracy. A UKF algorithm is implemented in [50] to estimate SOC using an improved ECM with a resistance and a capacitor correction factor. This was done to first, measure the effect of different current rates and the SOC estimation on the battery internal resistance, and secondly to identify the impact of different current rates and temperatures on the battery's capacity [51]. The works presented in [52, 53] use a multi-model approach that adopts a bank of EKFs to estimate the SOC of the battery. A robust extended Kalman filtering algorithm is implemented in [54] to be more robust to uncertainties in the system, and measurement equations, and noise covariances. A SOC estimation approach that uses an improvement in the measurement noise treatment is proposed in [55] and, by correcting the covariance matrix error in the depicted EKF, establishes an adaptive Kalman filtering algorithm that can reduce the estimation error. To deal with the variation of battery parameters due to temperature changes [56], an online approach is proposed for SOC estimation and parameter updating using a dual square root UKF based on unit spherical unscented transform.

To obtain a more accurate and reliable SOC, an improved Thevenin equivalent model is proposed and its parameters are identified. Experimental data results and simulated results are compared and analyzed to further appreciate the effectiveness of the improved adaptive extended Kalman filtering (AEKF) algorithm used. The use of the AEKF algorithm in this research is to accurately and diligently estimate the SOC and eliminate or reduce errors by updating the noise covariance matrix. The use of this adaptive extended Kalman filtering algorithm is an innovation in this work coupled with the 2RC Thevenin equivalent model for successful implementation and SOC estimation. According to the results realized, it is worth noting that, the SOC estimation using the AEKF algorithm is more accurate and reliable comparatively than the EKF algorithm. This paper is organized in sections as follows; The mathematical analysis is conducted in section 2, experimental analysis in section 3, and the last section is section 4 which coves conclusion and further research plan.

2. Mathematical Analysis

The basic concepts of SOC estimation, battery modeling, and the Kalman filtering algorithm are first introduced in this section. The improved Thevenin equivalent model including the 2RC's added as well as the description of corresponding parameters to be identified through experimentation are presented, the EKF and the improved AEKF algorithms are introduced in detail to emphasize the improvement in the SOC estimation accuracy.

2.1 The structure of the improved 2RC Thevenin equivalent model

An appropriate equivalent circuit model established and described, and the input, output, and state variables are determined. The modeling and simulation are done in Simulink/MATLAB and the parameters identified from the experimental data are used for real-time correction of variables like the internal resistor, capacitors, and current. Simulations are carried out and the results are verified to make sure the proposed method works perfectly for the accurate estimation of the SOC of the battery. The state of charge of the high-power lithium-ion battery is defined as the remaining capacity of the battery and is written mathematically as, the ratio of remaining capacity to the maximum available capacity and expressed as shown in Eq. (1).
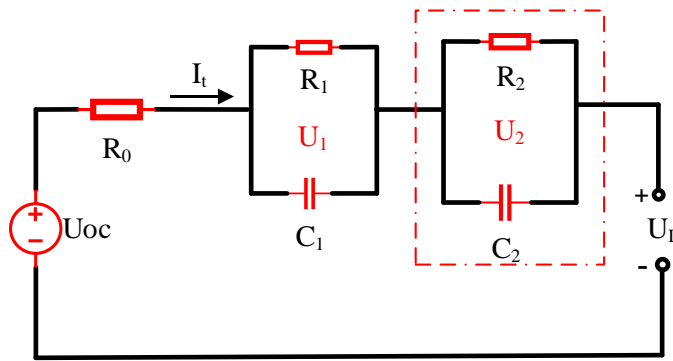
$$SOC_t = \frac{Q_t}{Q_0} \times 100\%$$
(1)

Where Q_t is the residual capacity of the battery at time t and Q_0 is the rated capacity. The value of SOC is the ratio between the current residual capacity and the capacity in the fully charged state when the battery is fully static at a certain time.

2.1.1 Electrical circuit model

The improved Thevenin equivalent circuit model is suggested for experimental and simulation purposes to model the behaviour of the high-power lithium-ion battery. The dynamic system of the Thevenin model describes the fixed parameters as variables that vary with the state of charge and temperature, enabling a more accurate description of the performance of the battery. This method was adopted because the topology generally proposes a tradeoff between battery cell computational requirements and the approximation of voltage precision. The model is as shown in (figure 1).

Figure 1: The 2RC Thevenin Equivalent Circuit Model

Where Uoc is the Open-Circuit Voltage, R_0 is the ohmic resistance of the battery, I_t is the charge/discharge current flowing from the voltage source and U_L represents the terminal voltage of the battery. R_1 and R_2 denote the electrochemical polarization resistance and concentration polarization resistance, respectively. C_1 and C_2 denote the electrochemical polarization capacitance and concentration polarization capacitance respectively.

2.1.2 State-space description

The state-space representation is a mathematical model of a physical system as a set of input, output, and state variables related to the first-order differential equations or difference equations. Concerning (figure 1) and the application of Kirchhoff's law, Eq. (2) is obtained and written as:

$$\begin{cases} U_L = U_{oc}(SOC) - i(t)R_0 - U_1 - U_2 \\ \dfrac{dU_1}{dt} = -\dfrac{U_1}{R_1 C_1} + \dfrac{i}{C_1} \\ \dfrac{dU_2}{dt} = -\dfrac{U_2}{R_2 C_2} + \dfrac{i}{C_2} \end{cases}$$
(2)

Where $[SOC, U_1, U_2]$ is selected as the state variables which need to be realized and after discretization of Eq. (2) and considering the definition of SOC as stated earlier, its state space equation can be written as shown in Eq. (3)

$$\begin{cases} \begin{bmatrix} SOC_{k+1} \\ U_{1,k+1} \\ U_{2,k+1} \end{bmatrix} = \begin{bmatrix} 1 & 0 & 0 \\ 0 & 1-T/\tau_1 & 0 \\ 0 & 0 & 1-T/\tau_2 \end{bmatrix} \\ U_{L,k+1} = U_{oc}(SOC, k+1) - U_1 - U_2 - IR_0 \end{cases}$$
(3)

In the above equation, parameters that the model needs to identify include ohmic internal resistance Ro, open circuit voltage Uoc, polarization internal resistance R_1, R_2, and polarization capacitor C_1 and C_2

which will lead to identifying U_1 and U_2.

2.2 Iterative calculation algorithms

2.2.1 Extended Kalman filtering

The extended Kalman filter algorithm is used for predicting the future state of a system based on a previous state. Kalman filter is a linear unbiased recursive filter, which is constantly "predicted and corrected" in the calculation process. Whenever new data is observed, new predicted values can be calculated at any time, which is very convenient for real-time processing. Due to the discharge rate, temperature, and complex internal chemical reaction, the battery presents a nonlinear state. Based on Kalman, the Jacobian matrix is obtained by using the Taylor formula for linearization, and the extended Kalman filter algorithm is obtained. The extended Kalman filter consists of two equations; state equations and observation equations, which include A, B, C, and D matrices that can be realized using Ro, R_1, R_2, C_1, and C_2. x_k is the system state matrix that captures the system dynamics and one of the matrix values represents SOC. The input of the system is u_k which is a control variable matrix that is known or can be measured. w_k, is the noise of the system state equation. Eq.. (4) shows the state equation and the observation equation.

$$\begin{cases} X_k = AX_{k-1} + BI_{L,k-1} + w_k \\ U_{L,k} = CX_k + DI_{L,k-1} + v_k \end{cases} \quad (4)$$

Where, x_k represents the system state variable at time k, y_k is the system observed variable at time k, u_k is the system input which is used as the control variable; A_k is the transfer matrix of state x from $k-1$ to k, and B_k is the input matrix. C_k is the measurement matrix, D_k is the feedforward matrix; ω_k is the noise of the system state equation. Kalman filter algorithm is used for state prediction and estimation. Kalman filter is mainly composed of five equations, which can be divided into the prediction stage and correction stage. The recursive relationship between the estimated value of state and covariance in the prediction stage (Time Update): is shown in Eq. (5).

$$\begin{cases} \hat{X}_k^- = \hat{X}_{k-1} + BI_{L,k-1} + w_k \\ \hat{P}_{k|k-1}^- = A\hat{P}_{k-1}A^T + Q_w \end{cases} \quad (5)$$

According to the model, the last moment of the state estimate of $k-1$, X_{k-1} and its covariance matrix P_{k-1} directly calculates the forecast of this moment, X_k^- and its covariance matrix $P_{k|k-1}$. Q_w is the covariance matrix of process noise w_k. The estimated values of Kalman gain are calculated as shown in Eq. (6).

$$K_k = \hat{P}_{k|k-1}^- C^T \left(C\hat{P}_{k|k-1}^- C^T + v_k \right) \quad (6)$$

The state correction stage is then performed for further computations to arrive at an appropriate equation that can be used to effectively make sure the appropriate parameters are identified. This can be achieved as shown in Eq. (7).

$$\begin{cases} \hat{X}_k = \hat{X}_k^- + K_t \left(U_{L,k} - C\hat{X}_k^- \right) \\ \hat{P}_{k|k-1} = \hat{P}_{k|k-1}^- - K_t C\hat{P}_{k|k-1}^- \end{cases} \quad (7)$$

The moment of state estimation x_k and $P_{k|k-1}$ is realized after this and the Kalman filter algorithm is completed in one iteration, and an iterative estimation is carried out for each observation, with good real-time performance.

2.2.2 Adaptive extended Kalman filtering algorithm

Currently, the SOC estimation method is mainly based on the equivalent model combined with the Kalman filter algorithm and its extended algorithm as well as fuzzy logic and neural network-related algorithms. The Kalman filter (KF) algorithm is one of the most widely used intelligent algorithms, and it is usually used in practical situations, such as path planning, target tracking, and SOC estimation of lithium-ion batteries. The basic principle of the algorithm is to take the minimum mean square error as the best estimation criterion, and by establishing a state equation and an observation equation model, a state-space model of signals and noise is used to introduce the relationship between the state variables and the observed variables. Time estimates and observations of the current time, update the estimates of the state variables. The Kalman filter is a mathematical function that provides estimating states with iterative steps, in a way to minimize the mean squared error. This technique has been providing performance efficiency in the field of parameter estimation and state transition. The improved Thevenin equivalent circuit model of the lithium-ion battery can be simplified as shown in Eq. (8).

$$\begin{cases} x_{k+1} = f(x_k, u_k) + w_k \ldots = A_k x_k + B_k u_k + w_k \\ y_k = h(x_k, u_k) + v_k \ldots = C_k x_k + D_k u_k + v_k \end{cases} \quad (8)$$

The functions f (*) and h (*) are nonlinear equations and the first equation is the state equation, where x_k is the n-dimensional system state vector at time point k, and v is the n-dimensional system noise vector. The function $f(x_k, u_k)$ is a non-linear state transition function. The second equation is an observation equation, where y is an observation vector, and v is a multi-dimensional system interference vector at time point k. The function $h(x_k, u_k)$ is a non-linear measurement function. The above function can be explored by using the Tailor method on the prior estimation point x_k of the state x_{k+1}. The higher-order components of the process can be ignored, and linear approximations of off (*) and h (*) can be used as shown in Eq. (9).

$$\begin{cases} f(x_k,u_k) \approx f(x_{k|k-1},u_k) + \dfrac{\partial f(x_k,u_k)}{\partial x_k}\Bigg|_{x_k = x_{k|k-1}} (x_k - x_{k|k-1}) \\[4mm] h(x_k,u_k) \approx h(x_{k|k-1},u_k) + \dfrac{\partial h(x_k,u_k)}{\partial x_k}\Bigg|_{x_k = x_{k|k-1}} (x_k - x_{k|k-1}) \end{cases} \tag{9}$$

The estimation process of the Kalman filter algorithm includes a time update and measurement update. The time update process is also known as the forecast process. It is a one-step prediction of the current state variable and provides a prior estimation process for the next moment. The measurement update process is the process of feeding back observations and correcting deviations. The EKF algorithm equations are as follows.

1. The filter initial conditions given in terms of the one-step prediction means the first state prediction has the same statistics as the initial condition of the system. The initial condition of the filter equation is given as:

$$x_0 = E(x), P_0 = \text{Var}(x) \tag{10}$$

2. When EKF is used to estimate the SOC of the lithium-ion battery, the SOC is a component of the state vector, the current is used as control quantity in the input parameters and the output is terminal voltage. The state vector estimation time update is given as:

$$x_{k|k-1} = f(x_{k-1},u_{k-1}) \tag{11}$$

3. The state covariance time update process predicts the current state variables by updating them and providing a prior estimate of the next time. State covariance update time update is given as:

$$P_{k|k-1} = FP_{k-1}F^T + Q_k \tag{12}$$

4. The Kalman gain is the relative weight given to the measurements and current state estimate and can be manipulated to achieve a particular performance. The calculation of the Kalman gain coefficient is given as:

$$K_k = P_{k|k-1}H^T(HP_{k|k-1}H^T + R_k) \tag{13}$$

5. The measurement update process, also known as the correction process, is a process of feedback on the observed values and the correction of the deviation. The state vector measurement update is given as:

$$x_k = x_{k|k-1} + K_k(y_k - h(x_{k|k-1},u_k)) \tag{14}$$

6. The state covariance matrix consists of the variances associated with each of the state estimates obtained and the correlation between the errors in the state estimates. The update state covariance matrix is given as:

$$P_k = (I - K_k H)P_{k|k-1} \tag{15}$$

In the above equations, $x_{k|k-1}$ is the direct time estimate at time k, x_{k-1} is the optimal estimate state value at the last moment. P_k is the covariance update of x_k, Q_k is the covariance of process noise w, K_k is the Kalman gain coefficient. R_k is the covariance of observation noise v. Since the covariance matrix P_k is decomposed, at least it is guaranteed that P_k is always non-negative definite, which can overcome the filter divergence caused by the limited word length of the computer. Sage-Husa algorithm adaptively updates the noise variables by comparing the final and initial estimated values. The estimator-related quantities are calculated as shown in Eq. (16).

$$\begin{cases} \tilde{y}_k = y_k - h(x_k,u_k) - R_{k-1} \\[2mm] Q_k = \dfrac{1}{k}\sum_{i=0}^{k-1}\left(K_k \tilde{y}_k \tilde{y}_k^T K_k^T + P_k - FP_{k|k-1}F^T\right) \\[2mm] R_k = \dfrac{1}{k}\sum_{i=0}^{k-1}\left(\tilde{y}_k \tilde{y}_k^T - HP_{k/k-1}H^T\right) \end{cases} \tag{16}$$

To make the estimation of noise more accurate and to avoid the influence of the observed value on the estimated value, this paper considers the noise at the previous moment and the current moment at the same time. In practice, the smaller the value of b, the smaller the impact at the previous moment; if the value of b is small, the estimated noise will oscillate, so it can be determined according to the specific situation. Then the calculation of the noise matrix is as shown in Eq. (17).

$$\begin{cases} Q_k = (1-d_{k-1})Q_{k-1} + d_{k-1}\left(K_k \tilde{y}_k \tilde{y}_k^T K_k^T + P_k - FP_{k/k-1}F^T\right) \\[2mm] R_k = (1-d_{k-1})R_{k-1} + d_{k-1}\left(\tilde{y}_k \tilde{y}_k^T - HP_{k/k-1}H^T\right) \end{cases} \tag{17}$$

2.2.3 Iterative calculation process
After obtaining the main parameters in the 2RC

Thevenin equivalent circuit model, the state space equation is obtained using the relationship between

voltage and current as shown in Eq. (18).

$$\begin{cases} E(\text{t}) = U_L + R_1 I(t) + u(t) \\ I(t) = \dfrac{u(t)}{R_2} + C\dfrac{du}{dt} \\ SOC(t) = SOC(t_0) - \dfrac{1}{Q_0}\displaystyle\int_{t_0}^{t} \eta i(t)\,dt \end{cases} \quad (18)$$

The three equations above are combined and discretized to obtain the state equation needed to perform further calculations leading to the conversion of non-discretized parameters into discretized ones as shown in Eq. (19).

$$\begin{cases} x(k|k-1) = A_k x(k-1) + B_k i_{k-1} + w_k \\ A_k = \begin{pmatrix} 1 & 0 \\ 0 & e^{-t/\tau} \end{pmatrix} \\ B_k = \begin{pmatrix} -\dfrac{t}{Q_0} \\ R_2(1-e^{-t/\tau}) \end{pmatrix} \end{cases} \quad (19)$$

It is important to also consider the observation equation for further successful computation and attainment of accurate results. The next thing to do therefore is the observation equation which is shown in Eq. (20).

$$y_k = h\left(x_{k-1}, i_{k-1}\right) + v_k = U_{oc} - R_1 i_k - u_k + v_k \quad (20)$$

The parameters of the battery are initially non-linear variables and have to be linearized. After linearization, using the first-order Taylor series with the values of A_k, B_k, and C_k, the formulas are obtained as shown in Eq. (21).

$$\begin{cases} \hat{A}_k = \begin{pmatrix} 1 & 0 \\ 0 & e^{-t/\tau} \end{pmatrix} \\ \hat{B}_k = \begin{pmatrix} -\dfrac{t}{Q_0} \\ R_2(1-e^{-t/\tau}) \end{pmatrix} \\ C_k = \begin{pmatrix} \dfrac{\partial u_{oc}}{\partial s_{oc}}, -1 \end{pmatrix} \end{cases} \quad (21)$$

In performing the mathematical calculation for the algorithm, there are a few steps to follow to achieve this. The first step is known as the state prediction stage. The predicted value at time k is calculated as shown in Eq. (22).

$$x(k|k-1) = A_{k-1}x(k-1) + B_{k-1}i_{k-1} \quad (22)$$

The second step in this calculation is the prediction of the covariance matrix. This is done by calculating the estimation error of $x(k|k-1)$, the covariance matrix of the corresponding $x(k|k-1)$ is obtained as shown in Eq. (23).

$$P(k \mid k-1) = A_{k-1}\hat{P}_{k-1}A_{k-1}^T + Q_k \quad (23)$$

The Kalman gain is calculated in the third step to further improve the computation and arrive at the value for a specific time. The Kalman gain at time k is obtained as shown in Eq. (24).

$$K_k = P_k C_k^T (C_k P_k C_k^T + R_k)^{-1} \quad (24)$$

The fourth step is the update of the status. The optimal estimated value of the existing state is estimated from the real-time measured/obtained open-circuit voltage value Uoc(k) as shown in Eq. (25).

$$\hat{X}_k = x(k|k-1) + K_k\left[U_{oc}(k) - C_k * x(k|k-1)\right] \quad (25)$$

In the fifth step, the noise covariance is updated. The noise covariance is updated according to the Kalman gain. This helps to avoid errors or at least minimize them and leads to accurate estimation. The noise covariance of the previous moment is shown in Eq. (26).

$$\hat{P}_k = (1 - K_k C_k)P_k \quad (26)$$

In the calculation, the five steps are continually cycled in a loop, and the estimated state is continuously updated so that the estimated value is closer to the true value during the update process. The basic iterative calculation process for SOC is as shown in (figure 2).
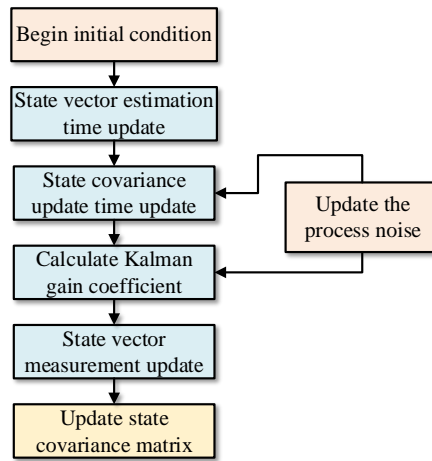
Figure 2: The SOC estimation process using the AEKF algorithm

2.3 Model building and Realization

2.3.1 Simulink/MATLAB Simulation model

After obtaining the required circuit model parameters, the simulation model of the lithium-ion battery is established in Simulink/MATLAB. The simulation model has mainly composed of the SOC calculation module, the circuit parameter updating module, and the terminal output voltage calculation module. The SOC calculation module is based on the extended Kalman filtering algorithm and the Improved Adaptive extended Kalman filtering algorithm. SOC values are obtained through the use of the codes for calculations based on the algorithms and to prevent the battery from overcharge and over-discharge. In this work, the influence of temperature change on the output voltage of the lithium-ion battery is ignored. For the time-domain ordinary differential equation of the 2RC Thevenin equivalent circuit, the corresponding voltage response equation is solved and discretization as it is required before modeling to obtain the discretization state-space equation of the model. The logical structure of the circuit model is shown in (figure 3).
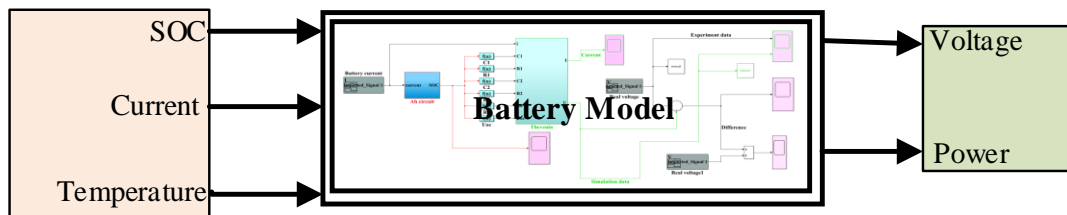
Figure 3: Logical structure of the circuit model

In the battery management system, both current and terminal voltage are input, as the battery simulation model is to verify the accuracy of the parameter settings in the model, the current is input and terminal voltage is the output. The simulation module can be built and the second-order RC internal circuit is the core part of the whole module, and the circuit structure is directly used to build the module, including an ohmic internal resistance, two RC parallel structures, a controllable voltage source, and controllable current source, voltage, and current sensor, and input and output interface, as shown in (figure 4).
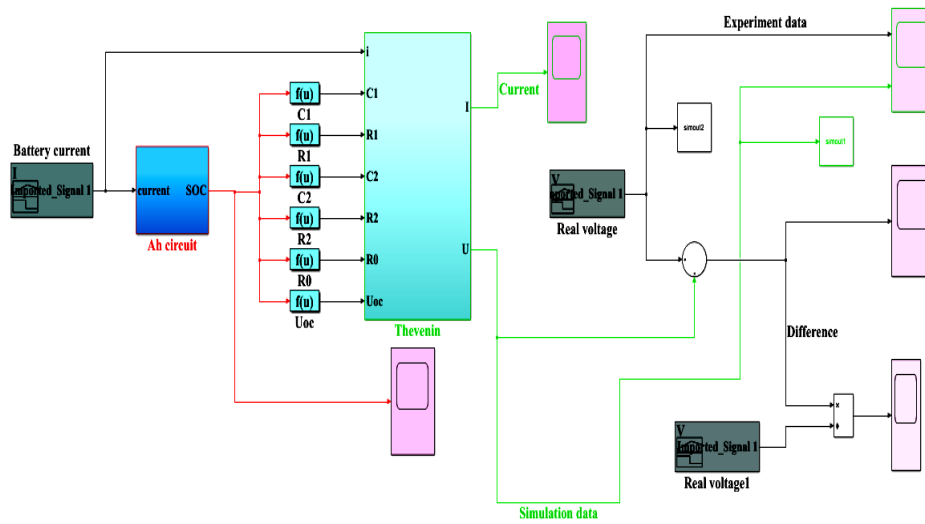
Figure 4: The Simulation Model of the 2RC Thevenin equivalent model

(Figure 5) shows the internal component of the model in (figure 4) representing the proposed 2RC Thevenin equivalent circuit model. The necessary inputs and outputs are labeled and other components are duly presented in the figure based on the proposed model.
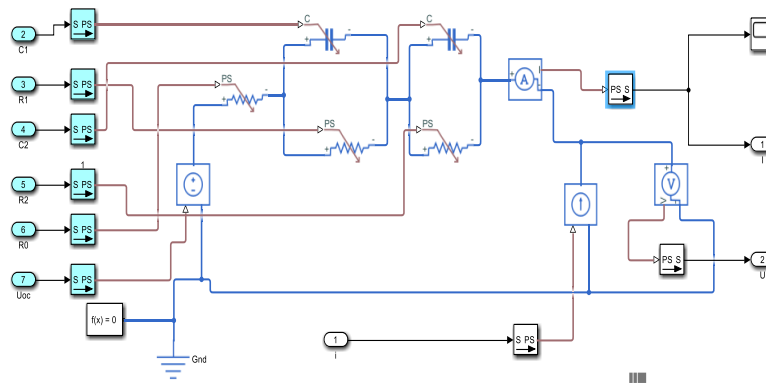

Figure 5: The internal circuit of the 2RC Thevenin equivalent model

Controllable voltage source and controllable current source are the signal interface in SIMULINK, which can turn the signal into a material port. Convert the external input voltage source into a voltage and current source that the circuit can connect to. Voltage sensors and current sensors are also signal transducers, converting physical interfaces into signal interfaces. The extended Kalman filtering algorithm and the Adaptive extended Kalman filtering algorithm are coded into the simulation model and the complete diagram is shown in (figure 6).
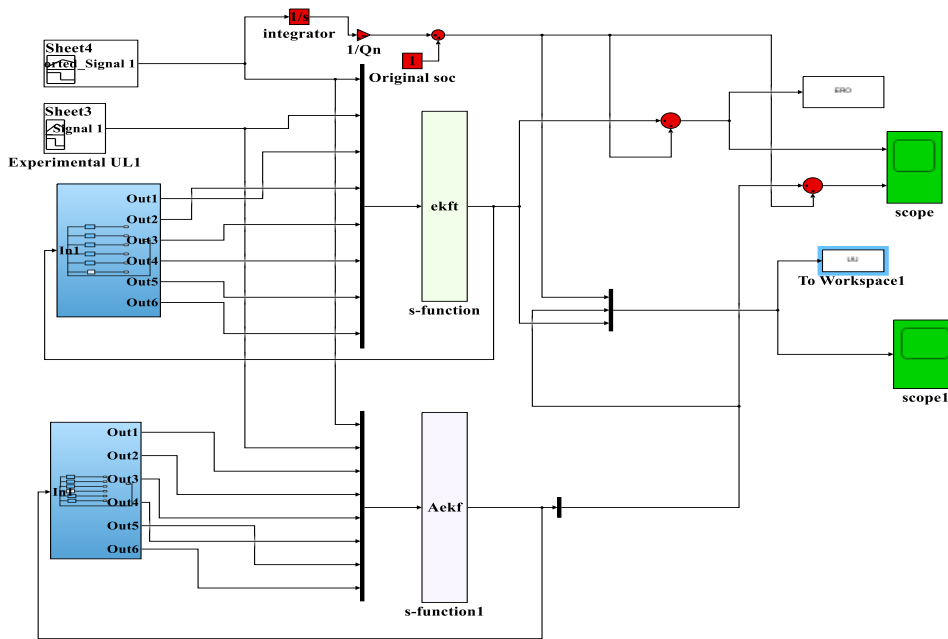
Figure 6: Integration of algorithms into the simulation diagram

3. Experimental Analysis
3.1 Test platform construction

The GTK 3.7V 40Ah high-power lithium-ion battery was used for this experiment with a rated capacity of 40 Ampere hour (Ah), a charge cut-off voltage of 4.2V, and a discharge cut-off voltage of 2.75V. The test equipment is the sub-source BTS 750-200-100-4, with a maximum charge-discharge power of 750W, a maximum voltage of 200V, and a maximum current of 100A. The basic properties of the battery are shown in table 1.

Table 1: Basic technical parameters of the battery

Factor	Specification
Size: length * width * height/ mm	148×27×92
Rated voltage/V	3.7
Maximum load current /A	5C
Rated capacity/Ah	40
Charge cut-off voltage/V	4.2
Discharge cutoff voltage/V	2.75

Setting up the experiment requires the connection of the battery to the test machine which is also connected to a computer. A specific terminal is chosen from the 16 available, and connect to the battery for the experiment to commence. The software on the computer is then programmed to follow a logical algorithm to accomplish the task.
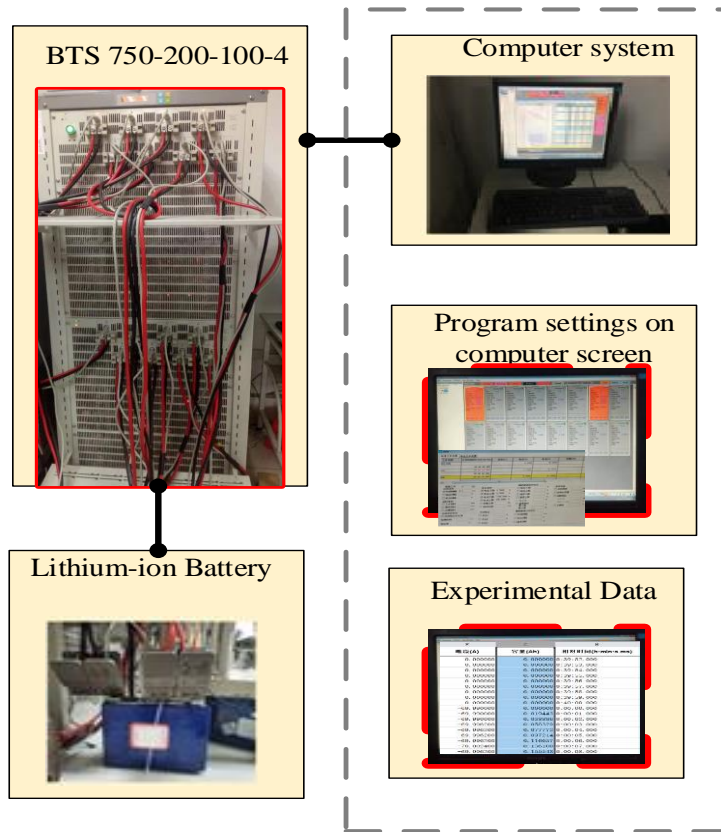
Figure 7: Experimental Setup

3.2 Results, verification, and comparison

3.2.1 Parameter identification and extraction
The Open-Circuit Voltage test:

The open-circuit voltage (OCV) of the battery is the stable voltage value of the battery when the battery is left in the open circuit condition. The test was performed on the Lithium-ion battery to acquire data for parameter identification. Using the Ampere hour (Ah) method, the real capacity of the battery is determined and used in the programming during the experiment. After charging the battery, the battery terminal voltage will gradually decline to a stable value when it is left in the open circuit condition and after discharge, the battery terminal voltage will gradually rise to a stable value when the load is removed. The electromotive force of the battery is equal to the open-circuit voltage of the battery. The battery electromotive force is one of the metrics used to measure the amount of energy stored in the battery. The relationship between the battery OCV and the battery SOC can be attained through this experiment. There are a few ways to obtain the open-circuit voltage of a battery and include the stationary method, also known as the direct method which is relatively more accurate.

The program that controls the experiment which resides on a computer connected to the battery testing machine (BTS 750-200-100-4) is then set to follow conditions to obtain a flow chart of the processes involved in the experiment. The test consists of simple steps and follows a logical sequence with a loop that ensures continuity and data capture at relevant SOC points. The first step is the capacity test that calibrates the capacity of the battery and the subsequent steps capture the OCV of the battery at specific SOC points.
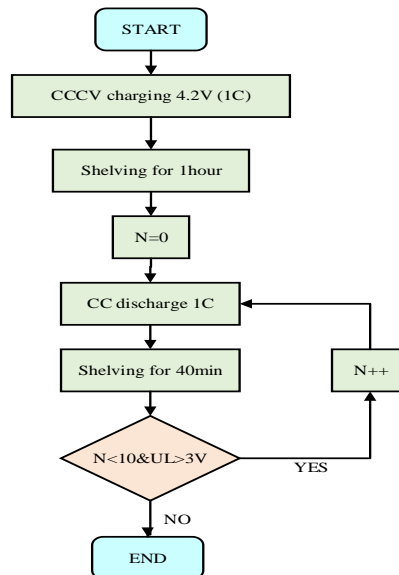
Figure 8: OCV experiment process

In the test, the measured voltages at the end of each standby stage are regarded as the final open-circuit voltage. All the values of the open-circuit voltages at different SOC's are measured and recorded. Table 2 shows the OCV data obtained at the various levels of SOC. These values were extracted and used for the curve fitting that reveals the relationship between OCV and SOC and further used to obtain the polynomial equation for further calculations.

Table 2: Values from the SOC/OCV test

SOC	1	0.9	0.8	0.7	0.6	0.5	0.4	0.3	0.2	0.1
OCV	4.1914	4.0628	3.9521	3.8529	3.7602	3.6852	3.6393	3.6188	3.5645	3.4886

The OCV/SOC values were imported and using the curve fitting tool, a relationship was realized through the use of a polynomial fitting. The variation of OCV with SOC obtained through the experimental method is shown in (figure 9).
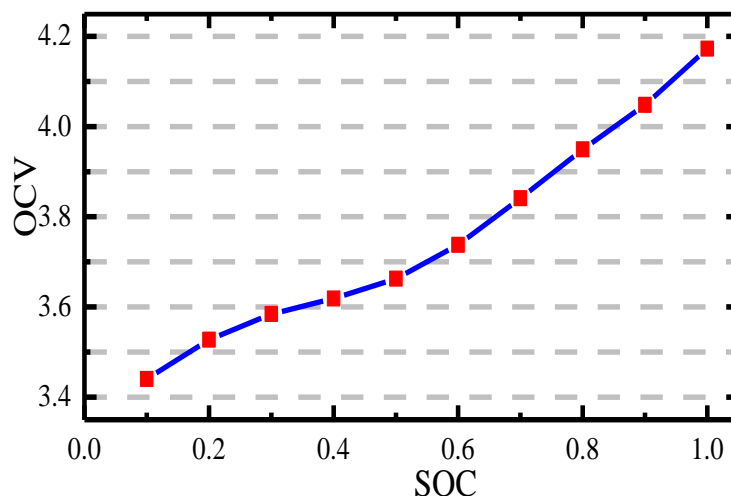

Figure 9: OCV/SOC Curve fitting

The capacity and Hybrid Pulse Power Characterization (HPPC) Test:

The experiment is performed as a method for parameter identification of the Thevenin model and then data from the test conducted is analyzed and used in equations to calculate the parameters. Taking the GTK 3.7V 40Ah high-power lithium-ion battery as the research object, the battery test equipment was is BTS750-200-100-4. The HPPC experiment was conducted on the lithium-ion battery according to the "American Freedom CAR battery experiment manual". The single HPPC working step was to take 1C (current 40A) constant current 10s, shelve for 40s, and 1C (current 40A) constant current charge 10s, and then shelve. The Capacity and HPPC experiments performed on the high-power lithium-ion battery were conducted according to the following steps.

1. The battery is fully charged using a constant current of 1C followed by a constant voltage of 4.2V. Then, the battery is discharged with a constant current to its discharge cut-off voltage of 2.75V. The experiment is repeated three (3) times for the difference between the discharge capacity of each measurement not to exceed 2%, and then the measured capacity is deemed to be the actual capacity of the battery.

2. The battery is left in the open-circuit condition to rest for 40 minutes to achieve electrochemical and heat equilibrium. After performing step (1) on the lithium-ion battery, SOC = 1.

3. Discharge the experimental battery at a constant current of 1C for 10s, leave it for 40s, and charge at 1C for 10s, then leave it.

4. Discharge the battery with a current value of 40A for 6 minutes to decrease the battery SOC to the next SOC point and leave it for 30 minutes.

5. Repeat steps (3) (4) 9 times to obtain the complete data for the test.

The HPPC test is carried out using simple steps in order to obtain the necessary values needed for parameterization and further computation as far as the research is concerned. The experimental process of the HPPC test can be seen in (figure 10).
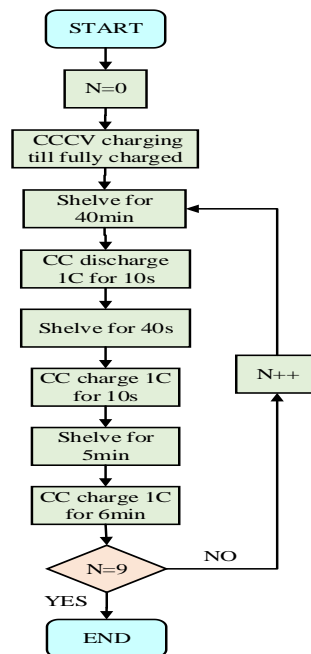

Figure 10: HPPC test process

Through parameter identification, the functional relations of resistance, capacitance, voltage, and SOC were obtained. Then, the circuit module was built in Simulink/MATLAB. The module contains other submodules that assist in the processing, calculation, and optimization of the interface for better simulation. The EKF and the improved AEKF algorithms were incorporated in this module as well. The parameters identified in the experiment and subsequent use in SOC estimation are compared with the results from the simulated. This can be obtained by simulating the construction and the design of function to operate on is completed. Through direct comparison of the curves, the error in parameter identification can be observed and manipulated by changing the value of parameter input, and the optimal simulation model can be obtained by modifying the functions.

The experimental results from the OCV and HPPC tests are used as the basis for parameterization. The test was conducted at 0.1 SOC intervals from 1.0 to 0.1. When a current I is loaded, a voltage rise or drop appears when there is a pulse charge or discharge and this can be used to calculate the parameters. (Figure 11) shows the test data for SOC at 0.9.
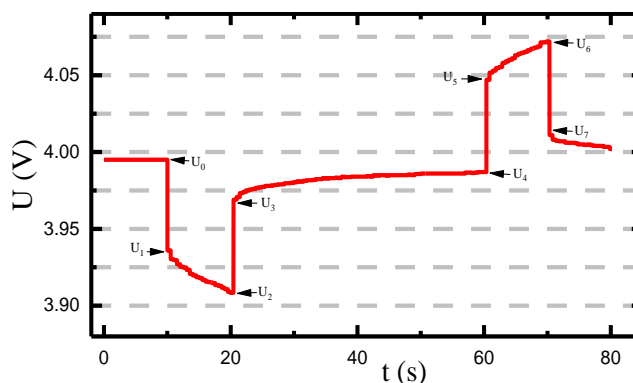
Figure 11: Voltage curve for a specific SOC

The labels U_0 to U_7 represent values for various segments of the curve corresponding to the battery during the experiment. U_0-U_3 and U_4-U_7 show the discharge characteristics and charging characteristics of the battery respectively.

1. The U_0-U_1 segment shows the ohmic internal resistance Ro, which depicts the rapid drop of the voltage at the moment of discharge of the battery.

2. U_1-U_2 shows the steady drop in terminal voltage due to the polarization capacitor which is due to the polarization effect of the battery as it is being charged. This polarized capacitor is the zero-state response of the 2RC series loop.

3. U_2-U_3 shows the resting of the battery and the disappearance of the load current, the ohmic voltage disappears, and the rapid rise of the terminal voltage.

4. U_3-U_4 shows the steady rise of the terminal voltage as the polarization capacitance discharges through the polarization resistance, forming a zero-input response of the 2RC series loop.

The opposition to the flow of the current offered by the battery itself resulting in the generation of heat is measured in Ohms. Based on the voltage drop from U_0 to U_1 for each of the SOC's, the ohmic resistance R_0 can be deduced. The value of (R_1, R_2, C_1, C_2) as seen in the Thevenin equivalent circuit diagram is to

make it stable and achieve possible desired outcomes. Whenever the potential of an electrode is forced away from its value at the open-circuit, R_1 is calculated. This causes current to flow through electrochemical reactions that occur at the electrode surface. The value of R_1 can be determined using the voltage response of the battery cell to a discharging current pulse and voltage and can be calculated using the difference in voltage (U) over the current I. The build-up of solutes on the membrane surface due to convective-diffusive transport in the boundary layer which can be linked to R_2 can be determined and calculated using the difference in voltage (U) over the current I. A capacitor is formed when two conducting plates are separated by a non-conducting media called the dielectric. The value of the capacitance depends on the size of the plates, the distance between the plates, and the properties of the dielectric. The part of the polarization of the battery resulting from changes in the electrolyte concentration due to the passage of current through the electrode C_2 is determined.

With these equations, the information can be used to derive values of the parameters. This data can then be simulated in Simulink MATLAB for verification and validity of the values and the modeling of the 2RC Thevenin equivalent circuit. Table 3, shows the data acquired after the calculations.

Table 3. The model Parameter calculation result

SOC	OCV/V	Ro/mΩ	R_1/mΩ	R_2/mΩ	C_1/10^3 F	C_2/10^3 F
1.0	4.1914	0.0324	0.0642	0.0578	20.3215	19.2359
0.9	4.0628	0.0307	0.0532	0.0635	20.7558	19.2560
0.8	3.9521	0.0474	0.0508	0.0657	21.3673	20.2565
0.7	3.8529	0.0474	0.0635	0.0732	21.6135	20.6354
0.6	3.7602	0.0542	0.0676	0.0770	22.6417	19.6580
0.5	3.6852	0.0568	0.0730	0.0793	23.0131	22.0827
0.4	3.6393	0.0603	0.0725	0.0840	22.1528	21.8318
0.3	3.6188	0.0603	0.0832	0.0872	22.3564	20.2624
0.2	3.5645	0.0604	0.0841	0.0765	21.0251	20.4528
0.1	3.4886	0.0661	0.0762	0.0818	23.2540	20.5187

The values of the internal Ohmic resistance R_0, the electrochemical polarization resistance R_1, and concentration polarization resistance R_2 calculated from the proposed 2RC Thevenin equivalent circuit are compared in (figure 12(a)). The values of the electrochemical polarization capacitance C_1 and the concentration polarization capacitance C_2 calculated from the 2RC Thevenin equivalent circuit are compared in (figure 12(b)).
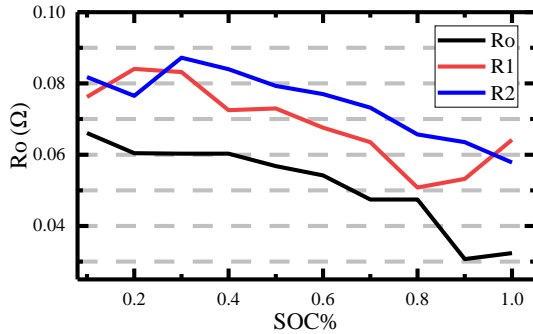

(a) Resistance identification result   **(b) Capacitance identification result**
**Figure 12: comparison of the identified parameters**
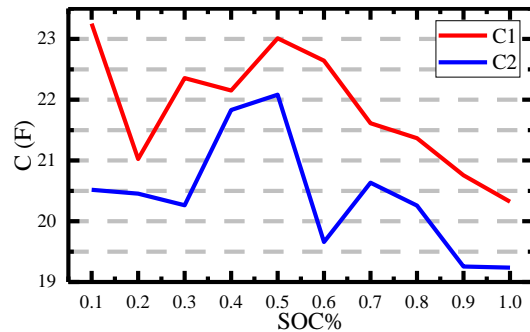
According to the result, it can be observed from (figure 12(a)) that, the internal resistance R_0 decreases steadily as state-of-charge increases. The electrochemical polarization resistance R_1 first increases and then decreases with an increasing SOC and then increases again as SOC approaches the highest point. The concentration polarization resistance R_2 first decreases then increases sharply and gently decreases as SOC increases. From (figure 12(b)), the results show the variation in the curves of the two capacitances are somewhat similar and seem to be fluctuating as SOC increases and finally decreases when SOC is above 0.7 till it reaches the highest point.
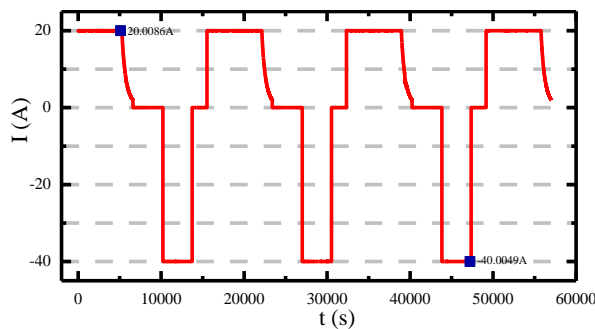
3.2.2 Capacity test result
The capacity experiment was conducted for calibration of the capacity, current, energy, and voltage of the battery. According to the capacity experiment, these various parameters can be deduced and compared with the information provided by the manufacturer to compare and see if the experiment was successful or not. (Figure 13(a)) is the Capacity variation curve with time and it can be deduced from the figure that the Capacity of the battery is approximately 40Ah. Three maximum values obtained in the experiment are 39.1360Ah, 39.2072Ah, and 39.2323Ah.
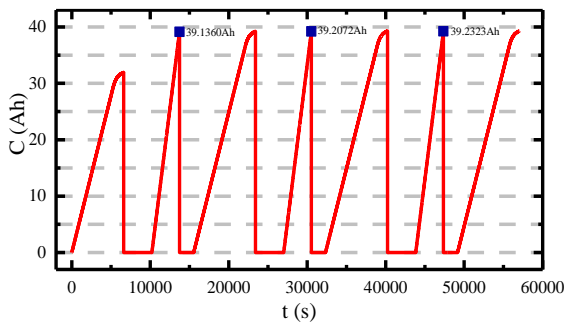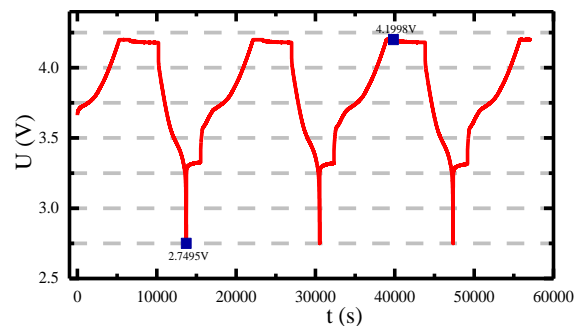

(a) Capacity variation curve
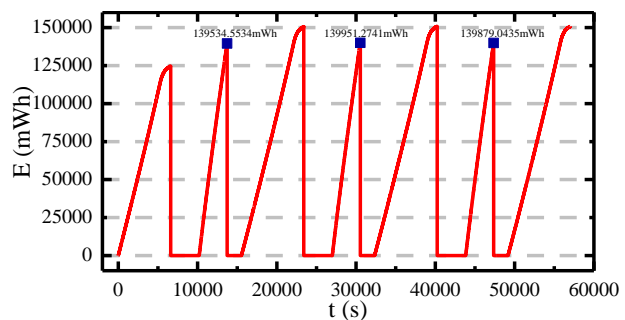
(b) Energy variation curve

(c) Current variation curve

(d) Voltage variation curve
Figure 13: capacity test results

Clarivate Analytics *indexed*

(Figure 13(b)) shows the energy variation curve and displays three maximum energy values obtained in the experiment as 139.534Wh, 139.951Wh, and 139.879Wh. The energy of the battery is therefore approximately 140Wh. The energy variation curve fluctuates in the whole process since its main purpose is to charge the lithium-ion battery when the constant-current charge-discharge interval is carried out. (Figure 13(c)) shows the current variation curve of the capacity test and displays the maximum and minimum current values obtained in the experiment as 20.0086A, and -40.0049A respectively. (Figure 13(d))

shows the voltage variation curve and displays the maximum and minimum values obtained in the experiment as 4.1998V which is approximately the maximum voltage of the battery stated as 4.2V and 2.7495V approximately 2.75V stated earlier as the minimum voltage of the battery.

The comparison of the current and voltage curves from the experiment and how the variation is depicted to achieve the capacity of the battery. The current flow and the voltage can be seen and analyzed from (figure 14).
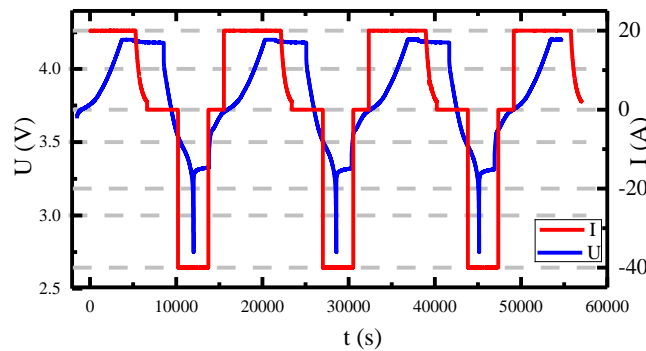

**Figure 14:Voltage/Current discharge variation curve**

3.2.3 HPPC test results

The result from the HPPC test was used to identify each OCV at specific SOC points. The voltage curve is also useful in the identification of battery parameters. (Figure 15(a)) and (b) shows the schematic diagram of the HPPC terminal voltage and

current curves with time respectively and illustrates the mechanism of the HPPC experiment throughout the test. The figure also emphasizes one of the SOC points for reference and shows the single charge and discharge variation in the experiment.
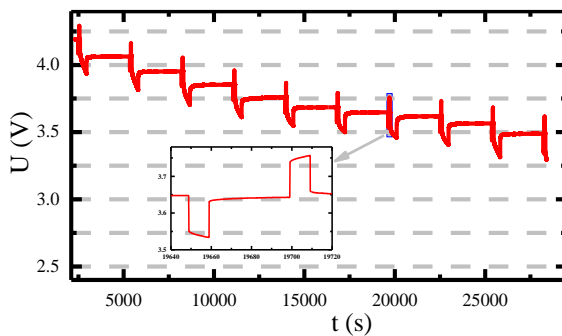
(a) Voltage variation curve
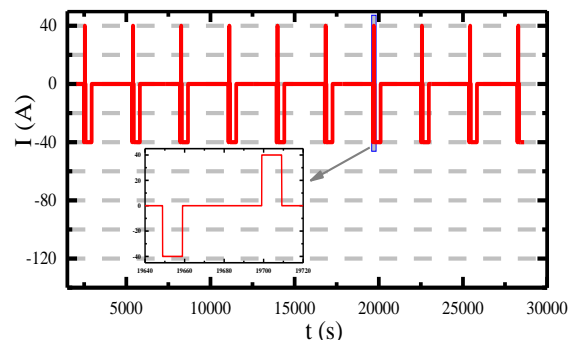
(b) Current variation curve

Figure 15: HPPC test result

From the result, it can be observed that as the number of cycles increases, the battery terminal voltage assumes a downward trend. The current variation reveals that, as the number of cycles increases, the discharge current increases. (Figure 16)

shows the comparison of the voltage and current curves from the HPPC experiment and the variation with time. The overlaying curves shown in the figure depict the real or actual occurrence with the battery at specific times.
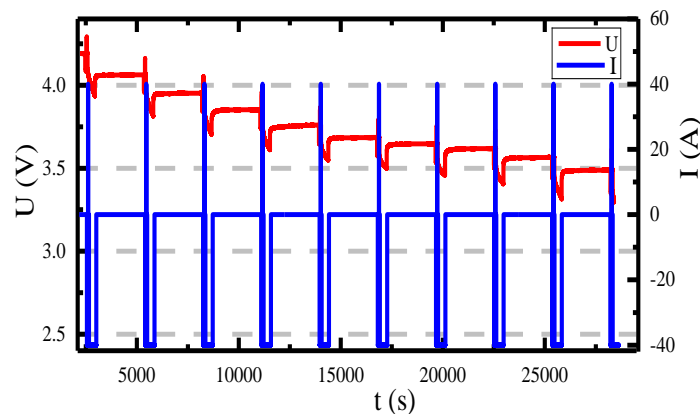
Figure 16: Voltage/Current discharge variation curve

3.2.4 SOC estimation result

The experimental results and parameterization did then used for SOC estimation. (Figure 17) shows the estimation depicting a downward slope with time as SOC reduces from 1 to 0.1. The result shows a gradual decrease and fluctuating trend which is because there is a process of alternating charge and discharge during the experiment with the discharge time longer than the charging time.
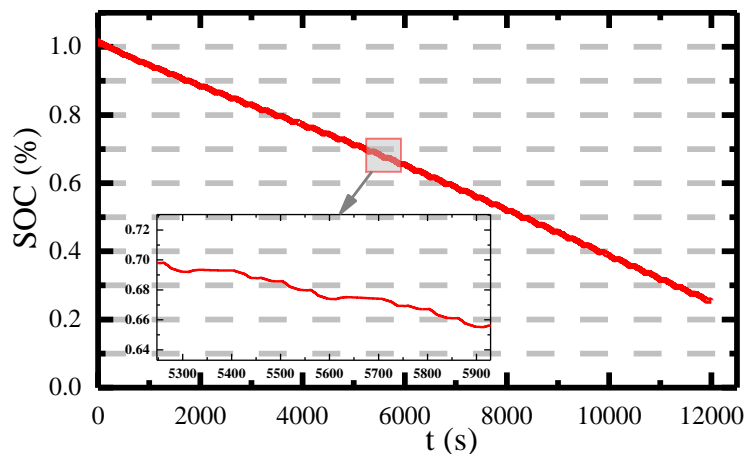

Figure 17: SOC variation curve

3.3 Verification of research results

3.3.1 Voltage characteristics

The 2RC Thevenin equivalent circuit model is established through parameterization with the HPPC experimental results. To verify the validity of the SOC estimated values in the simulation, the results are compared with and the results from the HPPC experiment and the computations done thereafter. The value of current (I) in the experimental data obtained by the test equipment is taken as the input condition, and the simulation terminal voltage is obtained through the simulation model and the experimental terminal voltages are compared to obtain the results as shown in (figure 18).
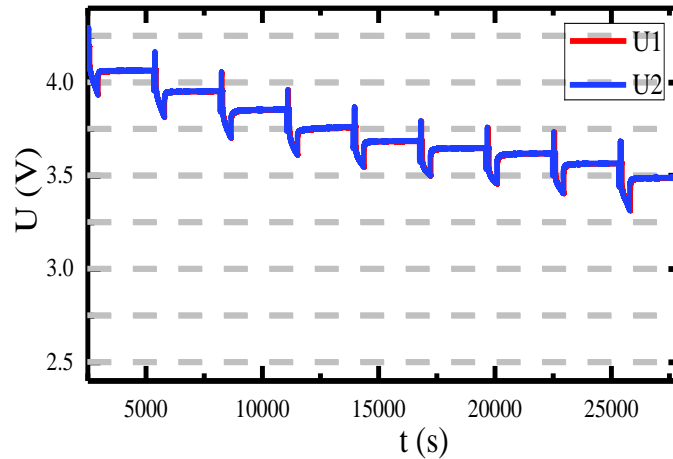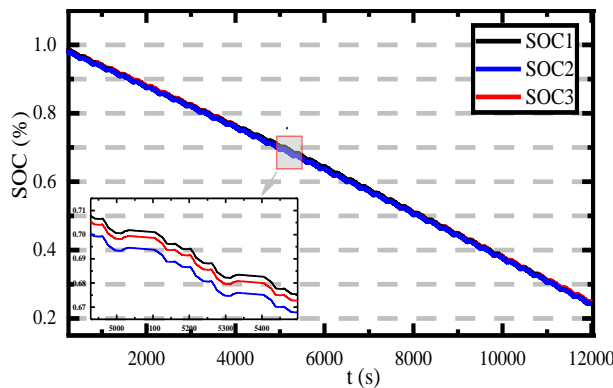
Figure 18: Comparison of voltage variation curves

Where U1 is the change curve of real terminal voltage data obtained through the HPPC test while U2 is the output terminal voltage curve obtained through the simulation model. The figure shows the variation trend of both the experiment and simulation curves is similar to that of the actual test curve. This means that the results can be verified and authenticated as appropriate for use in any calculation toward the accurate estimation of SOC.

3.3.2 Comparison and Verification of SOC estimation result

To illustrate the adaptability and performance of the improved adaptive Kalman filtering algorithm, for SOC estimation, Beijing Bus Dynamic Stress Test (BBDST) working condition experiment was designed and the effectiveness of the algorithm for accurate SOC estimation was compared with the extended Kalman filtering algorithm. SOC estimation results from the proposed model and the use of the two algorithms; the extended Kalman filtering algorithm and the adaptive extended Kalman filtering algorithm are then compared to assess and verify the validity and efficient performance of the model and algorithms implemented. The three methods are compared as shown in (figure 19). It can be observed from the figure that the three methods all follow the same trend and have a good convergence. The same figure also shows the difference in error margin comparing the use of the EKF and the AEKF estimation curves with that of the true SOC curve.

(a). comparison of SOC estimation curves
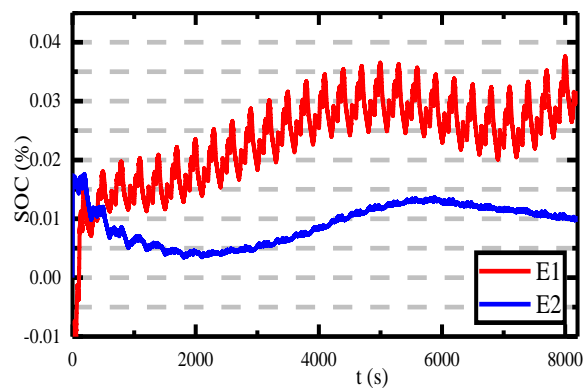
(b). SOC estimation Error

Figure 19: SOC variation curves for three different methods

(Figure 19(a)) is the result of SOC estimation for three different methods. SOC1 is the true SOC value, and SOC2 is the SOC estimate using the extended Kalman algorithm and SOC3 is the SOC estimation using the adaptive extended Kalman filter. (Figure 19(b)) is the error curve obtained through the difference in SOC values of the two algorithms. The error of SOC estimation using the extended Kalman is around 4.97%, and the error of SOC estimation using the improved adaptive extended Kalman algorithm is less than 1.85% and has a strong correction function.

In recent years, researchers have proposed some new estimation methods to help correct the errors with especially the traditional SOC estimation methods. The use of these improved and adaptive methods would reduce the estimation errors as much as possible and improve the estimation accuracy. In the actual battery management system, the methods to estimate the SOC of the battery are all traditional, and most of these new methods are only in the theoretical

research or simulation stage.

4. Conclusions and Further Research Plan

In the quest to improve the accuracy and reliability of the lithium-ion battery state of charge estimation in this study, the 2RC Thevenin model was established and the parameters were obtained. This model was used due to its advantages of low error, long-term testing, and accounting for polarization effects and transient analysis for power battery charging and discharging. The steps used in the experiment were simple and convenient, and the algorithm complexity, very moderate making the experimental results obtained accurate and appropriate for parameterization. The maximum relative errors of the 2RC Thevenin equivalent models using both algorithms were all less than 4.97%, which can generally satisfy the precision requirements for practical engineering calculation, such as algorithms based on ECM for advanced BMSs. The choice of an adaptive law for the process noise covariance matrix shows an improvement in estimation performances. In terms of maximum estimation error, the EKF result was 4.97%, while with AEKF this range reduced up to 1.85%. The extended Kalman filter algorithm used effectively reduces the influence of nonlinear equations and successfully realizes the SOC estimation of the battery. The improved adaptive extended Kalman filter algorithm for SOC estimation used in this work can effectively and accurately estimate the battery SOC and has high precision compared to the extended Kalman algorithm. The results are of great instructional significance to the application in practical control systems for the equivalent circuit modeling of batteries. The improved adaptive extended Kalman filter algorithm has good convergence speed, higher estimation accuracy, and stability and is appropriate and convenient for SOC estimation. Therefore, for stringent applications such as automotive and high-power demanding devices, the second-order RC model could be the preferred choice, and the use of an adaptive algorithm for SOC estimation would be better for accurate and timely information.

For further and future research, it is important to perform several experiments to acquire necessary experimental data for analysis. It is also important to use several methods and techniques in the estimation of SOC. The use of algorithms is also an important aspect of research in this direction because it helps to improve the accuracy of SOC estimation. These algorithms have been improved over the years and more improvement and research leading to the establishment of more effective and efficient algorithms must be promoted to better the function of Battery management systems for estimations.

Acknowledgments

References:

1. Yang, J., et al. (2018). Online state-of-health estimation for lithium-ion batteries using constant-voltage charging current analysis. *Applied Energy*, 212: pp. 1589-1600.
2. Hesse, H.C., et al. (2017). Lithium-ion battery storage for the grid—A review of stationary battery storage system design tailored for applications in modern power grids. *Energies*, 10(12): p. 2107.
3. Ali, M.U., et al. (2019). Towards a smarter battery management system for electric vehicle applications: A critical review of lithium-ion battery state of charge estimation. *Energies*, 12(3): p. 446.
4. Lai, X., Zheng, Y., & Sun, T. (2018). A comparative study of different equivalent circuit models for estimating state-of-charge of lithium-ion batteries. *Electrochimica Acta*, 259: pp. 566-577.
5. Liu, K., et al. (2019). A brief review on key technologies in the battery management system of electric vehicles. *Frontiers of Mechanical Engineering*, 14(1): pp. 47-64.
6. Cacciato, M., et al. (2017). Real-Time Model-Based Estimation of SOC and SOH for Energy Storage Systems. IEEE *Transactions on Power Electronics*, 32(1): pp. 794-803.
7. Beirão, M.D., et al. (2016). *Balancing management system for improving Li-ion batteries capacity usage and lifespan.* in 2016 IEEE 16th International Conference on Environment and Electrical Engineering (EEEIC).
8. Ali, U.M., et al. (2019). Towards a Smarter Battery Management System for Electric Vehicle Applications: A Critical Review of Lithium-Ion Battery State of Charge Estimation. *Energies*, 12(3).
9. Feng, Y., et al. (2016). Intelli*gent battery management for electric and hybrid electric vehicles: A survey.* in 2016 IEEE International Conference on Industrial Technology (ICIT).

10. Tang, X., Liu, B., & Gao, F. (2017). State of Charge Estimation of LiFePO4 Battery Based on a Gain-classifier Observer. *Energy Procedia*, 105: pp. 2071-2076.

11. Wei, X., Yimin, M., & Feng, Z. (2019). Lithium-ion Battery Modeling and State of Charge Estimation. *Integrated Ferroelectrics,* 200(1): pp. 59-72.

12. Rivera-Barrera, P.J., Muñoz-Galeano, N., & Sarmiento-Maldonado, O.H. (2017). SoC Estimation for Lithium-ion Batteries: Review and Future Challenges. *Electronics*, 6(4).

13. Venugopal, P. (2019). State-of-Health Estimation of Li-ion Batteries in Electric Vehicle Using IndRNN under Variable Load Condition. *Energies*, 12(22).

14. Blaabjerg, F., Dragicevic, T., & Davari, P. (2019). Applications of Power Electronics. *Electronics*, 8(4).

15. Zhang, K., et al. (2019). Parameter Identification and State of Charge Estimation of NMC Cells Based on Improved Ant Lion Optimizer. *Mathematical Problems in Engineering*, 2019: p. 18.

16. Su, J., et al. (2019). An equivalent circuit model analysis for the lithium-ion battery pack in pure electric vehicles. *Measurement and Control*, 52(3-4): pp. 193-201.

17. Qin, D., et al. (2019). Modeling and Simulating a Battery for an Electric Vehicle Based on Modelica. *Automotive Innovation*, 2(3): pp. 169-177.

18. Tian, Y., et al. (2019). Performance analysis and modeling of three energy storage devices for electric vehicle applications over a wide temperature range. *Electrochimica Acta*, 2019: p. 135317.

19. Saldaña, G., et al. (2019). Analysis of the Current Electric Battery Models for Electric Vehicle Simulation. *Energies*, 12(14).

20. Mendoza, S., et al. (2016). Optimization and experimental validation of a thermal cycle that maximizes entropy coefficient fisher identifiability for lithium iron phosphate cells. *Journal of Power Sources*, 308: pp. 18-28.

21. Rothenberger, M.J., et al. (2015). Genetic optimization and experimental validation of a test cycle that maximizes parameter identifiability for a Li-ion equivalent-circuit battery model. *Journal of Energy Storage*, 4: pp. 156-166.

22. Zhang, C., et al. (2018). Online estimation of battery equivalent circuit model parameters and state of charge using decoupled least squares technique. *Energy*, 142: pp. 678-688.

23. Xu, Y., et al. (2020). State of charge estimation for lithium-ion batteries based on adaptive dual Kalman filter. *Applied Mathematical Modelling*, 77: pp. 1255-1272.

24. Writer, B. (2019). M*odels, SOC, Maximum, Time, Cell, Data, Parameters, in Lithium-Ion Batteries: A Machine-Generated Summary of Current Research, B. Writer, Editor.* Springer International Publishing: Cham. (pp. 195-247).

25. Serhan, H.A., & Ahmed, E.M. (2018). *Effect of the different charging techniques on battery life-time:* Review. in 2018 International Conference on Innovative Trends in Computer Engineering (ITCE).

26. Jarraya, I., et al. (2019). An online state of charge estimation for Lithium-ion and supercapacitor in hybrid electric drive vehicle. *Journal of Energy Storage*, 26: p. 100946.

27. Barai, A., et al. (2015). A study of the open circuit voltage characterization technique and hysteresis assessment of lithium-ion cells. *Journal of Power Sources*, 295: pp. 99-107.

28. Zhang, C., et al. (2016). A Generalized SOC-OCV Model for Lithium-Ion Batteries and the SOC Estimation for LNMCO Battery. *Energies*, 9(11).

29. Gao, Z.C., et al. (2017). State-of-Charge Estimation and Active Cell Pack Balancing Design of Lithium Battery Power System for Smart Electric Vehicle. *Journal of Advanced Transportation*, 2017: p. 14.

30. Wang, Q., et al. (2017). Correlation between the model accuracy and model-based SOC estimation. *Electrochimica Acta*, 228: pp. 146-159.

31. Yang, Q., et al. (2017). A simplified fractional order impedance model and parameter identification method for lithium-ion batteries. *PloS one*, 12(2): p. e0172424-e0172424.

32. Guangming, L., et al. (2014). *A comparative study of equivalent circuit models and enhanced equivalent circuit models of lithium-ion batteries with different model structures.* in 2014 IEEE Conference and Expo Transportation Electrification Asia-Pacific (ITEC Asia-Pacific).

33. Yang, J., et al. (2017). Improved Battery Parameter Estimation Method Considering Operating Scenarios for HEV/EV Applications. *Energies*, 10(1).

34. Xia, B., et al. (2016). Accurate Lithium-ion battery parameter estimation with continuous-time system identification methods. *Applied Energy*, 179: pp. 426-436.

35. Jiang, B., et al. (2017). Online Reliable Peak Charge/Discharge Power Estimation of Series-Connected Lithium-Ion Battery Packs. *Energies*, 10(3).

36. Parvini, Y., Vahidi, A., & Fayazi, S.A. (2018). Heuristic Versus Optimal Charging of Supercapacitors, Lithium-Ion, and Lead-Acid Batteries: An Efficiency Point of View. *IEEE Transactions on Control Systems Technology*, 26(1): pp. 167-180.

37. Raszmann, E., et al. (2017). *Modeling stationary lithium-ion batteries for optimization and predictive control. in* 2017 IEEE Power and Energy Conference at Illinois (PECI).

38. Lin, N., Ci, S., & Wu, D. (2016). *A novel low-cost online state of charge estimation method for reconfigurable battery pack.* in 2016 IEEE Applied Power Electronics Conference and Exposition (APEC).

39. Huria, T., Ludovici, G., & Lutzemberger, G. (2014). State of charge estimation of high power lithium iron phosphate cells. *Journal of Power Sources*, 249: pp. 92-102.

40. Xiao, T., et al. (2019). *Comparative Study of EKF and UKF for SOC Estimation of Lithium-ion Batteries.* in 2019 IEEE Innovative Smart Grid Technologies - Asia (ISGT Asia).

41. Liu, F., Ma, J., & Su, W. (2019). Unscented Particle Filter for SOC Estimation Algorithm Based on a Dynamic Parameter Identification. *Mathematical Problems in Engineering,* 2019: p. 14.

42. Chemali, E., et al. (2018). State-of-charge estimation of Li-ion batteries using deep neural networks: A machine learning approach. *Journal of Power Sources*, 400: pp. 242-255.

43. Jiménez-Bermejo, D., et al. (2018). Using Dynamic Neural Networks for Battery State of Charge Estimation in Electric Vehicles. *Procedia Computer Science*, 130: pp. 533-540.

44. Ma, Y., et al. (2016). Fractional modeling and SOC estimation of lithium-ion battery. IEEE/CAA *Journal of Automatica Sinica*, 3(3): pp. 281-287.

45. Jung-Hyo, B., & Bai, Z. (2016). *The development of technology on reduces the SOC error rate using Hybrid Kalman Filter(HKF) and the demonstration its performance using BMS platform.* in 2016 IEEE Transportation Electrification Conference and Expo, Asia-Pacific (ITEC Asia-Pacific).

46. Nejad, S., Gladwin, D.T., & Stone, D.A. (2015). *Enhanced state-of-charge estimation for lithium-ion iron phosphate cells with flat open-circuit voltage curves.* in IECON 2015 - 41st Annual Conference of the IEEE Industrial Electronics Society.

47. Liu-Henke, X., Scherler, S., & Jacobitz, S. (2017). *Verification oriented development of a scalable battery management system for lithium-ion batteries.* in 2017 Twelfth International Conference on Ecological Vehicles and Renewable Energies (EVER).

48. Peng, S., et al. (2017). State of Charge Estimation of Battery Energy Storage Systems Based on Adaptive Unscented Kalman Filter With a Noise Statistics Estimator. *IEEE Access*, 5: pp. 13202-13212.

49. Partovibakhsh, M., & Liu, G. (2015). An Adaptive Unscented Kalman Filtering Approach for Online Estimation of Model Parameters and State-of-Charge of Lithium-Ion Batteries for Autonomous Mobile Robots. *IEEE Transactions on Control Systems Technology*, 23(1): pp. 357-363.

50. Tian, Y., et al. (2014). A modified model based state of charge estimation of power lithium-ion batteries using unscented Kalman filter. J*ournal of Power Sources*, 270: pp. 619-626.

51. Barai, A., et al. (2018). A study of the influence of measurement timescale on internal resistance characterisation methodologies for lithium-ion cells. *Scientific reports*, 8(1): pp. 21-21.

52. Nejad, S., Gladwin, D.T., & Stone, D.A. (2016). *On-chip implementation of Extended Kalman Filter for adaptive battery states monitoring.* in IECON 2016 - 42nd Annual Conference of the IEEE Industrial Electronics Society.

53. Xia, X., & Wei, Y. (2016). *Lithium-ion batteries State-of-charge estimation based on interactive multiple-model Extended Kalman filter.* in 2016 22nd International Conference on Automation and Computing (ICAC).

54. Zhou, W., & Hou, J. (2019). A New Adaptive High-Order Unscented Kalman Filter for Improving the Accuracy and Robustness of Target Tracking. *IEEE Access*, 7: pp. 118484-118497.

55. Zhang, Z., et al. (2017). SOC Estimation of Lithium-Ion Batteries With AEKF and Wavelet Transform Matrix. *IEEE Transactions on Power Electronics*, 32(10): pp. 7626-7634.

56. Aung, H., Low, K.S., & Goh, S.T. (2015). State-of-Charge Estimation of Lithium-Ion Battery Using Square Root Spherical Unscented Kalman Filter (Sqrt-UKFST) in Nanosatellite. *IEEE Transactions on Power Electronics*, 30(9): pp. 4774-4783.